

# VLM-AR3L: Vision-Language Models for Absolute and Relative Rewards in Reinforcement Learning

Kuan-Chen Chen<sup>1</sup>, Winston Chen<sup>1</sup>, Wei-Fang Sun<sup>2</sup> and Min-Chun Hu<sup>1</sup>

<sup>1</sup>Department of Computer Science, National Tsing Hua University

<sup>2</sup>NVIDIA AI Technology Center (NVAITC)

## Abstract

Designing effective reward functions remains a major challenge in reinforcement learning (RL), particularly in open-ended environments where task goals are abstract and difficult to quantify. In this work, we present VLM-AR3L, a framework that leverages Vision-Language Models (VLMs) to provide both absolute and relative rewards for RL. VLM-AR3L interprets an agent’s visual observations in the context of a natural language task goal, and learns both absolute and relative rewards from VLM-generated preference labels. The absolute reward model predicts scalar evaluations for individual states, while the relative reward model compares consecutive observations to infer progress or regression toward the task goal. Their integration combines the stability of state-based evaluation with the robustness of comparative supervision. We evaluate VLM-AR3L across benchmarks spanning classic control, manipulation, and open-world embodied tasks, with a particular focus on Minecraft given its visual complexity and long-horizon decision-making requirements. Experimental results show that VLM-AR3L consistently outperforms prior VLM-based reward learning methods. Videos and code are available on the project website: <https://vlm-ar3l.github.io/>.

## 1 Introduction

Designing effective reward functions remains a major challenge in reinforcement learning (RL) [Laud, 2004; Leike *et al.*, 2018; OpenAI, 2019; Gupta *et al.*, 2022]. This challenge is especially pronounced in open-ended or visually complex environments, where task goals are often abstract and difficult to specify precisely. For example, in open-world environments such as Minecraft, agents are often assigned high-level goals (e.g., “build a shelter”) that require long-horizon planning and semantic understanding, while intermediate states provide little explicit reward signal. As a result, hand-crafting reward functions in such settings is typically impractical, due to ambiguous objectives, sparse feedback, and the absence of privileged state information. To address this bottleneck, recent approaches have explored leveraging large pre-trained

models as sources of reward, enabling agents to learn from high-level task descriptions or multimodal alignment signals.

Large language models (LLMs) have been shown to provide structured code or textual feedback for RL agents in text-based or programmatic settings. However, these methods often rely on privileged state access or handcrafted programmatic interfaces, limiting their applicability in real-world visual domains. When working with visual observations, contrastive vision-language models (cVLMs) such as CLIP are widely used to compute similarity scores between observations and goals for reward shaping. While simple and scalable, these methods typically require task-specific fine-tuning or retraining to be effective across different domains.

To move beyond direct similarity-based alignment, preference-based reward modeling has emerged as a promising alternative. These methods learn reward functions by comparing observation pairs and inferring preferences that are typically obtained from human feedback or large pre-trained models. This formulation enables finer-grained feedback and greater robustness in visually diverse or ambiguous environments. For instance, RL-VLM-F [Wang *et al.*, 2024] leverages generative vision-language models (VLMs) to generate pairwise preferences, which are then used to train a reward model that assigns scalar values to individual states. We call this approach **absolute reward**. However, we observe that absolute reward signals can be inconsistent across training steps (Fig. 1), due to the continual exposure to newly encountered states as training progresses. These inconsistencies, in turn, make long-horizon tasks difficult to optimize. In particular, absolute reward formulations fundamentally collapse in cyclic task structures or under ambiguous state orderings. In these scenarios, progress cannot be uniquely defined by a global state ordering, a limitation illustrated in Fig. 2. To address these limitations, we propose VLM-AR3L (Fig. 3), a framework that leverages VLMs to provide both absolute and relative rewards in reinforcement learning, without requiring fine-tuning or access to privileged internal environment information. Our contributions are as follows:

- **Dual-reward Design:** We introduce a dual-reward framework that jointly learns absolute and relative reward from VLM-generated preferences, with the relative reward providing robustness to reward inconsistency during training (Fig. 1) and resolving tasks with ill-defined global state ordering (Fig. 2).

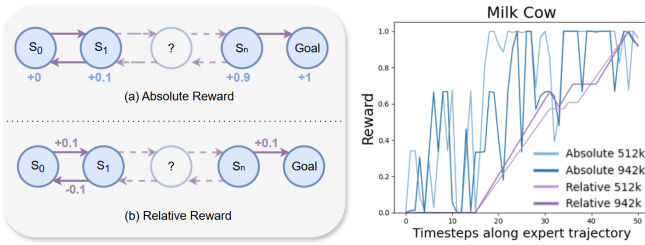


Figure 1: **Comparison of absolute and relative reward formulations.** **Left:** Conceptual illustration in a simple Markov process. Absolute reward assigns scalar values to states, where higher scores indicate proximity to the goal. Relative reward supervises transitions by assessing progress between state pairs. **Right:** Empirical reward trajectories evaluated along the same expert demonstration at different training steps (512k and 942k), showing that absolute reward varies substantially across training, whereas relative reward, after cumulative summation, exhibits greater temporal consistency.

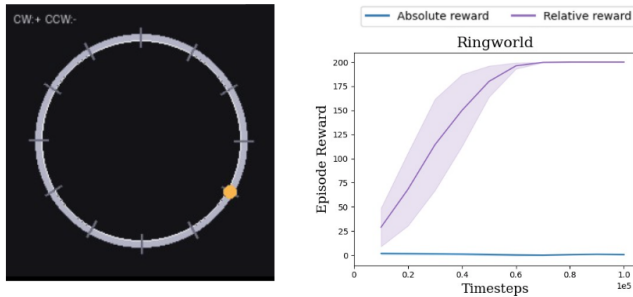


Figure 2: **RingWorld environment and reward comparison.** **Left:** Illustration of the RingWorld task, where the agent is required to move clockwise along a closed loop. **Right:** Learning curves for agents trained with absolute or relative reward, showing that absolute reward fails under the cyclic state ordering, whereas relative reward enables successful learning.

- **Relative reward modeling:** We train a Siamese network with VLM-generated preference supervision to model relative reward, avoiding repeated VLM inference during policy optimization, which substantially reduces computational overhead and improves performance.
- **Comprehensive evaluation:** We evaluate VLM-AR3L across diverse domains, including structured robotic control and open-ended tasks. VLM-AR3L consistently outperforms prior VLM-based methods and even surpasses carefully human-designed reward functions. We further conduct detailed ablation studies and VLM accuracy analyses to assess the reliability and scalability of our approach.

## 2 Related Work

**LLM-based Reward Learning.** Recent research has explored the use of large pre-trained models, particularly large language models (LLMs), as reward functions for reinforcement learning agents. LLM-based approaches have demonstrated the ability to generate structured code for downstream training [Ma *et al.*, 2024; Xie *et al.*, 2024; Wang *et al.*, 2023a;

Yu *et al.*, 2023; Wang *et al.*, 2023b], or to provide scalar reward signals from textual task descriptions in language-conditioned or text-based environments [Kwon *et al.*, 2023; Du *et al.*, 2023; Chu *et al.*, 2023]. However, many of these methods assume structured environments or require privileged state access, making them difficult to apply in high-dimensional, real-world visual domains. Additionally, for many open-ended or complex tasks, it is inherently challenging to specify reward logic in code, particularly when task-specific abstractions are involved or when full observability is lacking.

**CLIP-based Reward Learning.** When working with visual observations, a common strategy is to use CLIP-based vision-language models (cVLMs) to compute similarity-based scores between agent observations and language goals, typically via cosine similarity in the shared embedding space [Cui *et al.*, 2022; Adeniji *et al.*, 2023; Rocamonde *et al.*, 2024; Sontakke *et al.*, 2023; Mahmoudieh *et al.*, 2022; Palo *et al.*, 2023; Baumli *et al.*, 2024; Nam *et al.*, 2023]. While conceptually simple, these scores are often noisy and fragile, exhibiting high sensitivity to the phrasing of goals. To mitigate this, methods such as MineDojo [Fan *et al.*, 2022] and CLIP4MC [Jiang *et al.*, 2024] fine-tune CLIP on domain-specific datasets (e.g., Minecraft videos) to generate denser and more accurate reward signals. Other approaches like LIV [Ma *et al.*, 2023] and FuRL [Fu *et al.*, 2024] propose tailored fine-tuning procedures to enhance reward quality. While these methods reduce dependence on explicit ground-truth reward annotations, they typically require task-specific fine-tuning to capture subtle variations in visual input. Without fine-tuning, CLIP-based methods often fail to provide nuanced or reliable reward signals, limiting their generalization to new tasks or environments.

**Preference-based Reward Learning.** Beyond similarity-based rewards, recent works explore preference-based reward learning, which uses generative VLMs with multimodal reasoning capabilities, such as Gemini or GPT. A notable direction involves generating preference-based supervision without human labels. For instance, Constitutional AI [Bai *et al.*, 2022] and Motif [Klissarov *et al.*, 2023] use LLMs to produce preference labels or intrinsic rewards by comparing model outputs under high-level alignment principles. Extending this paradigm to the visual domain, RL-VLM-F [Wang *et al.*, 2024] proposes learning reward functions by querying vision-language models to compare agent observation pairs and generate preference labels, which are then used to supervise reward learning. Several follow-up works further explore the use of VLMs for visual preference modeling and feedback generation in various embodied environments [Venkataraman *et al.*, 2024; Ghosh *et al.*, 2025; Liu *et al.*, 2025]. However, these methods largely adopt absolute reward formulations, which are fundamentally limited in cyclic task structures or under ambiguous state orderings, where a consistent global ordering of states is difficult to define. Motivated by this limitation, we explore a dual-reward formulation that augments absolute rewards with relative rewards, aiming to improve robustness and scalability in complex, open-ended environments.

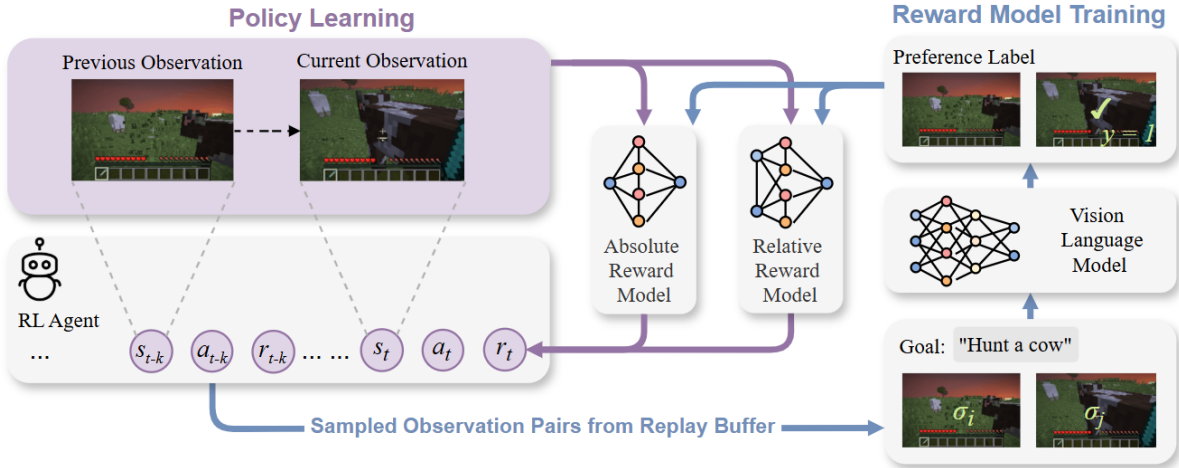


Figure 3: **Overview of the VLM-AR3L framework.** During reward model training (blue path), observation pairs are sampled from the agent’s replay buffer and evaluated by a VLM to determine which observation better aligns with the task goal. The resulting preference labels are used to supervise both absolute and relative reward models. During policy learning (purple path), the trained absolute model evaluates individual observations, while the relative model compares the agent’s current and previous observations to provide complementary absolute and relative reward signals.

### 3 Background

We consider a standard reinforcement learning (RL) setting modeled as a partially observable Markov decision process (POMDP) [Kaelbling *et al.*, 1998], defined by the tuple  $(\mathcal{S}, \mathcal{A}, \mathcal{T}, \mathcal{O}, \mathcal{R}, \gamma)$ . Here,  $\mathcal{S}$  denotes the set of environment states,  $\mathcal{A}$  denotes the set of possible actions,  $\mathcal{T}$  denotes the (unknown) state transition dynamics,  $\mathcal{O}$  denotes the observation space,  $\mathcal{R}$  denotes the reward function, and  $\gamma \in [0, 1)$  denotes the discount factor that prioritizes immediate rewards over long-term ones. At each time step  $t$ , the agent receives an observation  $s_t \in \mathcal{O}$  (e.g., an RGB image) and selects an action  $a_t \in \mathcal{A}$ , which causes the environment state in  $\mathcal{S}$  to evolve according to  $\mathcal{T}$ . The objective is to learn a policy  $\pi$  that maximizes the expected cumulative discounted reward over time.

**Preference-Based Reinforcement Learning.** Our work builds on the framework of preference-based reinforcement learning (pbRL), where agents learn reward functions from pairwise comparisons over trajectory segments or behavior snippets [Christiano *et al.*, 2017; Ibarz *et al.*, 2018; Lee *et al.*, 2021a; Lee *et al.*, 2021b]. In pbRL, a trajectory segment  $\sigma$  typically consists of a sequence of states  $\{s_1, \dots, s_H\}$ , where  $H$  denotes the sequence length of the segment. In this paper, we consider the special case that  $H = 1$ , as multi-image or video-based VLM reasoning remains less reliable in complex visual environments. Given a pair of segments  $(\sigma_i, \sigma_j)$ , an annotator provides a preference label  $y \in \{0, 1, -1\}$ , where  $y = 0$  indicates that  $\sigma_i$  is preferred,  $y = 1$  that  $\sigma_j$  is preferred, and  $y = -1$  that the two are equally preferable or incomparable. Given a reward function  $r$  over the states, we follow the standard Bradley-Terry model [Bradley and Terry, 1952] to compute the preference probability of a pair of segments:

$$\mathbb{P}[\sigma_i \succ \sigma_j] = \frac{\exp(r(s_i))}{\sum_{k \in \{i, j\}} \exp(r(s_k))}. \quad (1)$$

The reward model is then trained by minimizing a cross-entropy loss over a dataset of annotated preferences:

$$\mathcal{L}_{\text{reward}}(\theta) = -\mathbb{E}_{(\sigma_i, \sigma_j, y) \sim \mathcal{D}} \left[ \mathbb{1}_{\{y=0\}} \log \mathbb{P}_\theta[\sigma_i \succ \sigma_j] + \mathbb{1}_{\{y=1\}} \log \mathbb{P}_\theta[\sigma_j \succ \sigma_i] \right], \quad (2)$$

where  $\theta$  denotes the learnable parameters of the reward model.

In typical pbRL, the reward model and policy are trained iteratively: the reward model is updated using newly collected preference annotations, and the policy is optimized with standard RL algorithms using the learned reward model.

### 4 Method

Fig. 3 illustrates the overall architecture of the proposed VLM-AR3L framework. The training process consists of two intertwined pipelines: (1) reward model training and (2) policy learning. In the reward model training phase, observation pairs  $(\sigma_i, \sigma_j)$  are sampled from the agent’s replay buffer, along with a high-level language goal  $g$ . Each triplet  $(\sigma_i, \sigma_j, g)$  is passed to a frozen VLM, which outputs a preference label  $y$  indicating which observation better reflects progress toward the goal. These preference labels are used to supervise the training of both an **absolute reward model** and a **relative reward model**. During policy learning, the absolute reward model assigns state-based evaluations to the current observation  $s_t$ , while the relative reward model estimates progress by comparing the current observation  $s_t$  with a previous observation  $s_{t-k}$ , jointly providing dense and informative reward signals at each timestep. These signals guide the agent’s policy updates using standard reinforcement learning algorithms, eliminating the need for hand-crafted rewards or privileged state information.

## 4.1 Absolute Reward Model

Absolute reward models assign scalar values to individual states, where higher scores reflect states that are closer to the goal. As illustrated in Fig. 1, this state-based formulation provides a stable evaluation signal when a global ordering over the state space is well-defined, as each state is mapped to a fixed reward value independent of the agent’s trajectory.

Given a parameterized absolute reward function  $F_\psi^{\text{abs}}$  over the states, the model outputs a scalar reward value for each state following the formulation in Eq. (1):

$$F_\psi^{\text{abs}}(s_t) = r_\psi(s_t), \quad (3)$$

where  $r_\psi(s_t) \in \mathbb{R}$  denotes the absolute reward assigned to state  $s_t$ . The absolute reward at time step  $t$  is then given by:

$$R_\psi^{\text{abs}}(s_t) = F_\psi^{\text{abs}}(s_t). \quad (4)$$

## 4.2 Relative Reward Model

In contrast to the absolute reward model, the relative reward model evaluates progress between pairs of states. This design reduces reliance on a global understanding of the task space and improves robustness in partially observable or long-horizon scenarios. When new states are introduced and the reward models are updated, the relative reward of previously seen transitions remains stable. In contrast, absolute reward often suffers from instability, where earlier states may receive drastically different scores due to shifts in global normalization or value scaling (Fig. 1). Such robustness is especially beneficial in long-horizon settings, where consistent reward signals are essential for learning.

To implement the relative model, we employ a Siamese neural network [Bromley *et al.*, 1993] to learn a relative function  $F_\phi^{\text{rel}}$ . Given a pair of states  $(s_i, s_j)$ , the network outputs the preference probability:

$$F_\phi^{\text{rel}}(s_i, s_j) = \mathbb{P}_\phi[\sigma_i \succ \sigma_j]. \quad (5)$$

The relative model is trained using the same loss defined in Eq. (2). Architectural and training details are provided in the supplementary material (Appendix B.1).

During policy learning, the relative model aims to assess whether a transition indicates progress toward the goal  $g$ . To improve the model’s sensitivity to meaningful changes, particularly when consecutive observations are highly similar, we introduce a temporal offset  $k \geq 1$  and compare the current observation  $s_t$  with a past observation  $s_{t-k}$ . To ensure the reliability of the model’s predictions, we apply a symmetric confidence check. Specifically, a positive reward is assigned only if the model’s confidence in preferring  $s_t$  over  $s_{t-k}$  exceeds a threshold  $\tau$ , and the reverse prediction also indicates that  $s_{t-k}$  is not preferred over  $s_t$  with confidence exceeding  $\tau$ . This bidirectional check ensures both strong and consistent preference. Formally, the relative reward at time step  $t$  is computed as:

$$R_\phi^{\text{rel}}(s_t, s_{t-k}) = \begin{cases} 1, & \text{if } p_t^+ > \tau \text{ and } p_t^- < 1 - \tau, \\ -1, & \text{if } p_t^- > \tau \text{ and } p_t^+ < 1 - \tau, \\ 0, & \text{otherwise,} \end{cases} \quad (6)$$

where  $p_t^+ = F_\phi^{\text{rel}}(s_t, s_{t-k})$ ,  $p_t^- = F_\phi^{\text{rel}}(s_{t-k}, s_t)$ .

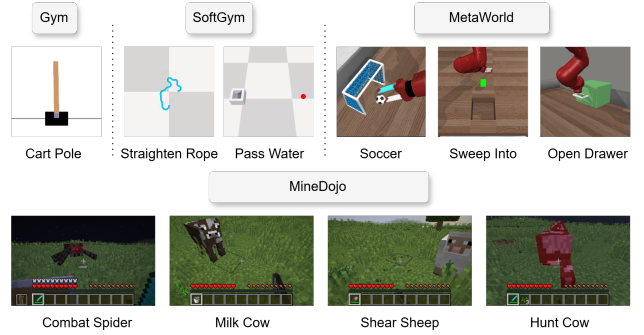


Figure 4: Environments and tasks used in our experiments, spanning structured control (Gym, SoftGym, MetaWorld) and open-ended visual domains (MineDojo).

## 4.3 Dual-Reward Design

Absolute and relative reward models offer complementary perspectives, balancing their individual strengths and weaknesses. Absolute rewards provide stable, state-based evaluations when a global ordering of the state space is well-defined, whereas relative rewards offer robust, transition-level supervision that remains reliable in cyclic, long-horizon, or partially observable settings. Motivated by this complementarity, we combine both reward signals to guide policy learning. The dual-reward is computed as:

$$R_{\psi, \phi}^{\text{dual}}(s_t, s_{t-k}) = \alpha R_\psi^{\text{abs}}(s_t) + (1 - \alpha) R_\phi^{\text{rel}}(s_t, s_{t-k}), \quad (7)$$

where  $\alpha$  is the weighting coefficient for the absolute reward signals, and both absolute and relative rewards are normalized to the same bounded range. Although the framework learns two reward models, both are trained using a single shared VLM querying pipeline. The VLM prompting strategy is described in Appendix A.1.

## 5 Experiments

### 5.1 Setup

**Environments and Tasks.** To assess the proposed VLM-AR3L, we conduct evaluations on ten tasks across four distinct environments (Fig. 4): *Cart Pole* from Gym [Brockman *et al.*, 2016]; *Straighten Rope* and *Pass Water* from SoftGym [Lin *et al.*, 2020]; *Soccer*, *Sweep Into*, and *Drawer Open* from MetaWorld [Yu *et al.*, 2019]; and *Combat Spider*, *Milk Cow*, *Shear Sheep*, and *Hunt Cow* from MineDojo [Fan *et al.*, 2022]. MineDojo, in particular, features long-horizon, open-ended tasks built on top of Minecraft. These tasks demand multi-step reasoning, complex object interaction, and semantic goal understanding, thereby posing significant challenges for visual reward learning. Collectively, these benchmarks encompass both structured robotic manipulation and expansive open-world scenarios, facilitating a comprehensive evaluation of VLM-AR3L’s generalization and adaptability. Detailed descriptions of the environments and tasks are provided in the Appendix C.

Model	Cart Pole	Straighten Rope	Pass Water	Soccer	Sweep Into	Drawer Open	Combat Spider	Milk Cow	Shear Sheep	Hunt Cow
Gemini-2.0-Flash [DeepMind, 2024]	<b>0.91</b>	<b>0.82</b>	0.70	<b>0.87</b>	<b>0.87</b>	<b>0.84</b>	0.82	0.78	0.80	<b>0.76</b>
GPT-4.1-nano [OpenAI, 2025]	0.66	0.81	0.65	0.60	0.81	0.65	0.64	0.62	0.66	0.66
Phi-3.5-Vision-Instruct [Abdin <i>et al.</i> , 2024]	0.56	0.67	0.62	0.52	0.69	0.54	0.63	<b>0.90</b>	<b>0.90</b>	0.66
MiniCPM-o-2.6 [OpenBMB, 2025]	0.53	0.61	<b>0.73</b>	0.65	0.79	0.56	0.59	0.61	0.62	0.64
DeepSeek-VL2-Tiny [Wu <i>et al.</i> , 2024]	0.50	0.50	0.50	0.50	0.50	0.56	<b>0.85</b>	0.68	0.66	0.67
Qwen2.5-VL-7B-Instruct [Team, 2025b]	0.50	0.76	0.70	0.55	0.52	0.67	0.64	0.59	0.72	0.64
InternVL2.5-8B [Chen <i>et al.</i> , 2025]	0.32	0.61	0.50	0.50	0.50	0.50	0.59	0.41	0.66	0.69
Gemma-3-12b-it [Team, 2025a]	0.52	0.51	0.50	0.50	0.50	0.50	0.50	0.50	0.54	0.50
CLIP (ViT-L/14@336px) [Radford <i>et al.</i> , 2021]	0.67	0.54	0.48	0.56	0.47	0.07	0.50	0.62	0.64	0.59
MineCLIP (Attn) [Fan <i>et al.</i> , 2022]	-	-	-	-	-	-	0.45	0.56	0.55	0.39

Table 1: Accuracy of different VLMs in predicting preference labels across tasks. Each task has 50 positive and 50 negative label queries.

Methods	Cart Pole	Straighten Rope	Pass Water	Soccer	Sweep Into	Drawer Open	Combat Spider	Milk Cow	Shear Sheep	Hunt Cow
GT Dense (Oracle)	1.00 ± 0.00	1.00 ± 0.00	1.00 ± 0.00	1.00 ± 0.00	1.00 ± 0.00	1.00 ± 0.00	0.99 ± 0.04	0.38 ± 0.15	0.67 ± 0.25	0.58 ± 0.33
GT Sparse (Oracle)	1.00 ± 0.00	1.00 ± 0.00	1.00 ± 0.00	1.00 ± 0.00	1.00 ± 0.00	1.00 ± 0.00	0.84 ± 0.10	0.37 ± 0.01	0.47 ± 0.09	0.15 ± 0.13
CLIP	1.00 ± 0.00	1.00 ± 0.00	0.00 ± 0.00	1.00 ± 0.00	0.67 ± 0.47	0.33 ± 0.47	0.59 ± 0.16	0.37 ± 0.00	0.40 ± 0.16	0.02 ± 0.02
MineCLIP	-	-	-	-	-	-	0.11 ± 0.09	0.31 ± 0.09	0.20 ± 0.00	0.09 ± 0.08
RL-VLM-F	1.00 ± 0.00	1.00 ± 0.00	1.00 ± 0.00	1.00 ± 0.00	1.00 ± 0.00	1.00 ± 0.00	0.53 ± 0.36	0.50 ± 0.32	0.47 ± 0.38	0.29 ± 0.22
<b>VLM-AR3L (Ours)</b>	<b>1.00 ± 0.00</b>	<b>1.00 ± 0.00</b>	<b>1.00 ± 0.00</b>	<b>1.00 ± 0.00</b>	<b>1.00 ± 0.00</b>	<b>1.00 ± 0.00</b>	<b>0.85 ± 0.05</b>	<b>0.95 ± 0.00</b>	<b>0.70 ± 0.10</b>	<b>0.52 ± 0.02</b>

Table 2: Success rate (mean ± standard error) of all evaluated methods across tasks. Results are averaged over 3 random seeds with 5 evaluation episodes per best checkpoint. MineCLIP is only evaluated on MineDojo tasks due to its domain-specific training.

**Baselines.** We evaluate our approach against several baselines that, like our framework, generate reward functions using only text goals and visual observations, without relying on privileged internal environment state information. In addition, we include oracle baselines using ground-truth rewards to assess whether VLM-generated rewards can serve as practical alternatives to human-designed reward functions.

- **RL-VLM-F [Wang *et al.*, 2024]:** A state-of-the-art preference-based method that queries a VLM for pairwise preferences between observations to train a scalar-valued reward function over individual states.
- **CLIP [Rocamonde *et al.*, 2024]:** A similarity-based method using cosine similarity between CLIP embeddings of the current observation and the language goal for reward shaping.
- **MineCLIP [Fan *et al.*, 2022]:** A domain-adapted CLIP variant fine-tuned on Minecraft videos, as proposed in MineDojo. Results are not directly comparable to the original paper, as self-imitation learning is omitted to ensure a fair and consistent training protocol across baselines.
- **GT Dense Reward (Oracle):** Hand-crafted, incremental reward functions based on full access to environment ground truth.
- **GT Sparse Reward (Oracle):** Binary success/failure signals given only at episode completion.

We exclude FuRL [Fu *et al.*, 2024], RoboCLIP [Sontakke *et al.*, 2023] and CLIP4MC [Jiang *et al.*, 2024] from our comparisons for the following reasons: FuRL relies on privileged reward signals, which falls outside our problem setting; RoboCLIP has been reported to perform poorly under comparable assumptions (as reported in RL-VLM-F); and CLIP4MC does not release its fine-tuned CLIP model, precluding an identical reproduction. Implementation details for all baselines are provided in Appendix D. For policy optimization, we employ Soft Actor-Critic (SAC) [Haarnoja *et*

*al.*, 2017] for Gym, SoftGym, and MetaWorld tasks, and Proximal Policy Optimization (PPO) [Schulman *et al.*, 2017] for MineDojo tasks, selected based on environment characteristics. Comprehensive training configurations and hyperparameters are detailed in the Appendix B.2.

## 5.2 VLM’s Label Accuracy

To assess the reliability of using VLMs as supervision, we evaluate several VLMs on multi-image reasoning across our tasks. For each task, we construct 100 image pairs with balanced pseudo preference labels (a 50/50 split) and prompt each VLM to identify the image that better aligns with the task goal.

Table 1 summarizes the accuracy of the tested VLMs across tasks. This evaluation serves to identify which models are most suitable as automated annotators for learning relative rewards. Gemini-2.0-Flash stands out for its consistently superior performance, achieving over 70% accuracy in all tasks, reflecting its robust multimodal reasoning capabilities. In contrast, GPT-4.1-nano underperforms relative to Gemini, showing noticeably lower accuracy across most tasks. Besides Gemini and GPT models, several open-source VLMs demonstrate competitive performance on specific tasks despite lacking general robustness. For example, Phi-3.5-Vision-Instruct achieves 90% accuracy on the Milk Cow and Shear Sheep tasks, while DeepSeek-VL2-Tiny excels in the Combat Spider task with an accuracy of 85%. MiniCPM-o-2.6 performs well in Pass Water, reaching 73%. On the other hand, CLIP and MineCLIP (evaluated only in MineDojo tasks) exhibit weak performance, underscoring their limitations in modeling multi-step interactions and temporal dependencies. Additional details and expanded evaluation results are provided in the Appendix A.2.

## 5.3 Comparison with Baselines

Building on the evaluation in Section 5.2, we adopt Gemini-2.0-Flash as the primary VLM for both VLM-AR3L and RL-VLM-F, given its consistently superior annotation performance across tasks. Table 2 reports the best success

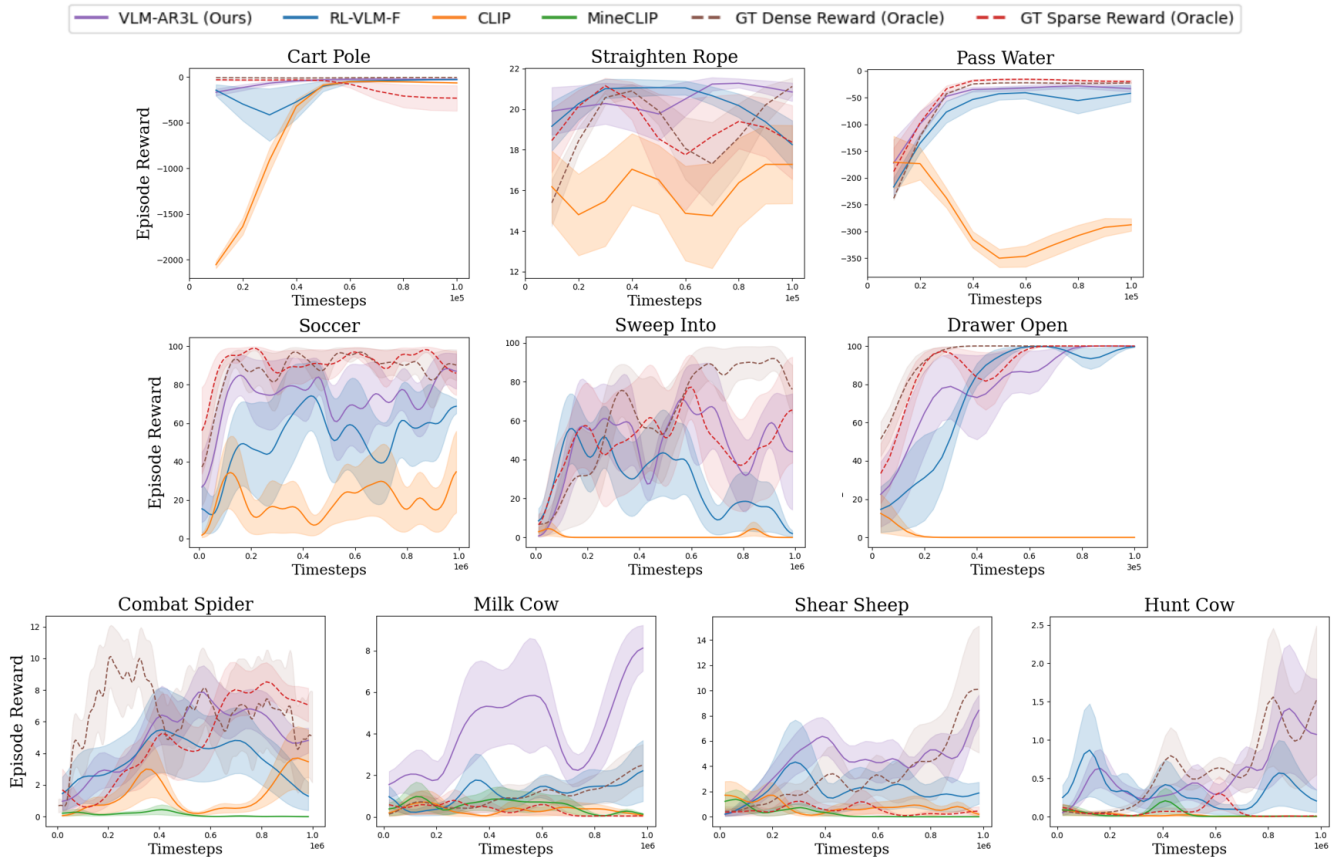


Figure 5: **Learning curves of all evaluated methods across tasks.** The x-axis represents training timesteps. The y-axis denotes episode rewards measured by the ground-truth dense reward. Results are averaged over 3 random seeds with 5 evaluation episodes per checkpoint. Shaded regions indicate standard error.

rates of all evaluated methods, and Fig. 5 presents the corresponding learning curves. We first examine similarity-based baselines such as CLIP and MineCLIP. While CLIP performs well in the low-dimensional Cart Pole environment, it struggles significantly in more complex environments. Notably, MineCLIP fails to generate reliable reward signals despite being fine-tuned on Minecraft videos. These results align with prior findings [Fu *et al.*, 2024; Jiang *et al.*, 2024; Wang *et al.*, 2024], suggesting that CLIP-based models often lack the granularity necessary to distinguish subtle visual differences, resulting in noisy and unstable reward signals during training.

Next, we evaluate RL-VLM-F, a preference-based method that learns scalar rewards over individual states. While RL-VLM-F achieves performance comparable to our method on simpler tasks, its efficacy degrades substantially in long-horizon and visually complex domains such as MineDojo. We attribute this degradation to its reliance on absolute state-based rewards, which requires a global understanding of the task space and often lacks robustness to novel or unseen state variations. In contrast, our proposed VLM-AR3L leverages relative comparisons between transitions, enabling it to generate more stable and goal-consistent rewards even as the state distribution evolves during training.

Finally, when compared against ground-truth dense and sparse rewards, our VLM-AR3L shows strong potential as a practical alternative. In most tasks, VLM-AR3L matches the performance of GT Dense Reward. Moreover, in tasks such as Milk Cow, Shear Sheep, and Hunt Cow, where GT Sparse Reward fails to provide sufficient guidance for learning, VLM-AR3L significantly outperforms the baseline, demonstrating its ability to handle sparse feedback and challenging long-horizon scenarios without requiring handcrafted rewards. These results underscore the practical applicability of our method for real-world settings where reward design is often infeasible.

## 5.4 Ablation Studies

**The Impact of VLM.** While Section 5.2 evaluates VLMs as annotators in terms of preference-label accuracy, we further study how the choice of VLM affects end-to-end RL performance when used to generate training supervision for VLM-AR3L. Specifically, we instantiate the same training pipeline and only vary the annotator VLM (Gemini-2.0, Phi-3.5, MiniCPM-o 2.6) across all tasks (Fig. 6 ; the full figures and table are provided in the Appendix E.2). Overall, the performance trends are broadly consistent with the label accuracy results in Section 5.2. While Phi-3.5 and MiniCPM-o 2.6

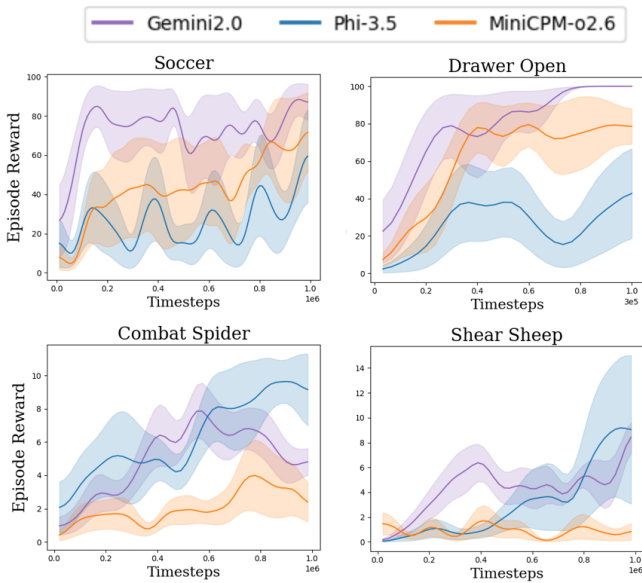


Figure 6: Ablation results with different vision-language models.

do not excel across all tasks, both exhibit clear task-specific strengths. Given their relatively small model sizes and open-source availability, they offer promising potential for broader adoption in future applications.

**The Impact of Relative Reward Architecture.** An alternative design choice for relative reward, instead of explicitly training a Siamese model (denoted as Siamese in Fig. 7), is to directly query a VLM at each timestep to evaluate progress (denoted as VLM-Direct). Another baseline derives relative rewards based on differences between absolute reward predictions (denoted as Abs-Diff). As shown in Fig. 7, explicitly training a Siamese model consistently outperforms direct VLM querying during rollouts (VLM-Direct). This improvement stems from preference-based training, which reduces noise in VLM judgments by learning a more stable comparison function, while also lowering computational overhead by avoiding repeated VLM queries at inference time (see Appendix B.3). We observe that computing relative rewards from absolute reward estimates (Abs-Diff) leads to inferior performance. This is because when the absolute reward model fails to assign reliable scores to individual states, the resulting differences become noisy and unreliable, leading to inaccurate relative assessments. We also examine the role of the symmetric comparison rule in Eq. (6) by evaluating a variant that omits this consistency check (Siamese w/o Sym). Removing the rule leads to notable performance drops across tasks, as it no longer filters inconsistent VLM judgments or prevents biased rewards when observations are visually similar.

**The Impact of Absolute and Relative rewards.** Fig. 8 (Full figures are provided in the Appendix E.3) analyzes how absolute and relative rewards contribute to each task. Absolute rewards are most beneficial in tasks with a well-defined global progress measure. In contrast, relative rewards become critical in tasks with ambiguous state ordering, cyclic struc-

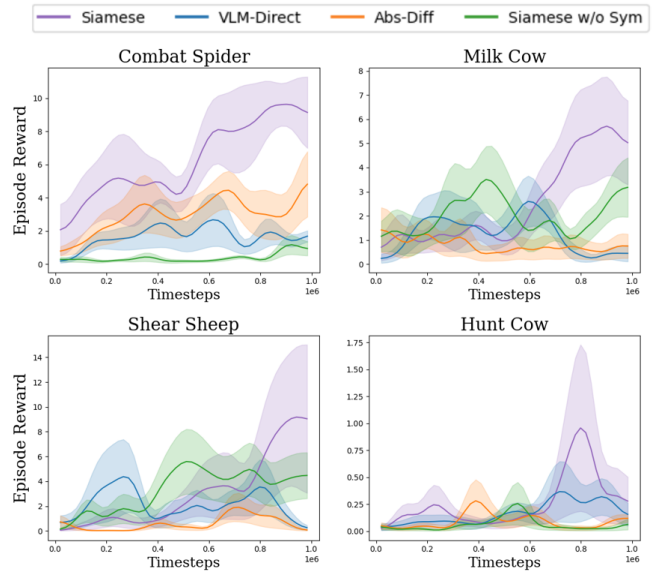


Figure 7: Ablation studies of the relative reward architecture across all experiments, using Phi-3.5 as the VLM.

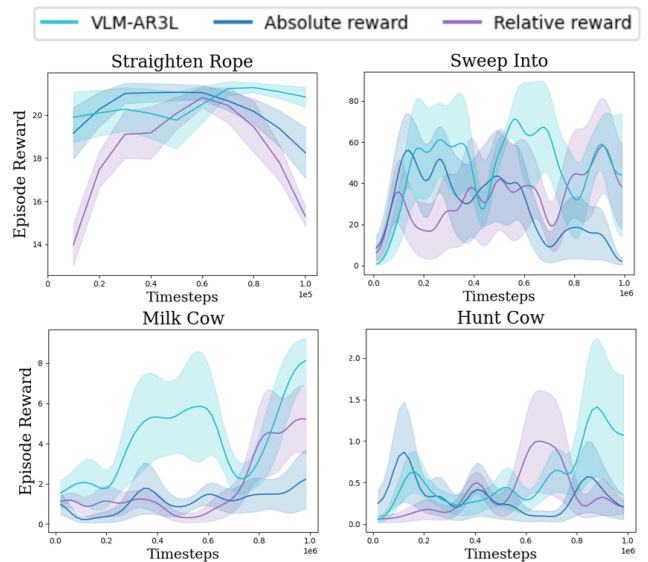


Figure 8: Ablation studies of absolute and relative rewards.

ture, or long-horizon exploration. Combining the two consistently leads to further improvements, indicating that the reward signals are complementary.

**The Impact of Hyper-parameters.** All results above are obtained using a single shared set of hyperparameters, with  $\alpha = 0.5$ ,  $\tau = 0.52$ , and  $k = 16$ , without task-specific tuning. We further confirm this robustness through hyperparameter ablation studies (see Appendix E.1), which show only minor performance variations.

## 6 Conclusion

Our results demonstrate that absolute and relative rewards provide complementary supervision for reinforcement learning with VLM-generated preferences. Absolute rewards are effective when a global notion of progress is well defined, while relative rewards are more robust in scenarios involving ambiguous, cyclic, or long-horizon state transitions. Integrating both reward types leads to more stable optimization and consistently outperforms existing VLM-based reward learning methods. Notably, in several tasks, our approach even surpasses manually engineered human reward functions.

## Acknowledgements

This research was funded by the National Science and Technology Council (NSTC) under grant numbers 114-2218-E-007-019. The last author was partially supported by the Hon Hai Research Institute. We express our sincere appreciation to the NVIDIA AI Technology Center (NVAITC) for the technical support and access to the Taipei-1 supercomputer.

## References

- [Abdin *et al.*, 2024] Marah Abdin, Jyoti Aneja, Hany Awadalla, Ahmed Awadallah, Ammar Ahmad Awan, Nguyen Bach, Amit Bahree, Arash Bakhtiari, Jianmin Bao, Harkirat Behl, Alon Benhaim, Misha Bilenko, Johan Bjorck, Sébastien Bubeck, Martin Cai, Qin Cai, Vishrav Chaudhary, Dong Chen, Dongdong Chen, Weizhu Chen, Yen-Chun Chen, Yi-Ling Chen, Hao Cheng, Parul Chopra, Xiyang Dai, Matthew Dixon, Ronen Eldan, Victor Fragoso, Jianfeng Gao, Mei Gao, Min Gao, Amit Garg, Allie Del Giorno, Abhishek Goswami, Suriya Gunasekar, Emman Haider, Junheng Hao, Russell J. Hewett, Wenxiang Hu, Jamie Huynh, Dan Iter, Sam Ade Jacobs, Mojan Javaheripi, Xin Jin, Nikos Karampatziakis, Piero Kauffmann, Mahoud Khademi, Dongwook Kim, Young Jin Kim, Lev Kurilenko, James R. Lee, Yin Tat Lee, Yuanzhi Li, Yunsheng Li, Chen Liang, Lars Liden, Xihui Lin, Zeqi Lin, Ce Liu, Liyuan Liu, Mengchen Liu, Weishung Liu, Xiaodong Liu, Chong Luo, Piyush Madan, Ali Mahmoudzadeh, David Majercak, Matt Mazzola, Caio César Teodoro Mendes, Arindam Mitra, Hardik Modi, Anh Nguyen, Brandon Norick, Barun Patra, Daniel Perez-Becker, Thomas Portet, Reid Pryzant, Heyang Qin, Marko Radmilac, Liliang Ren, Gustavo de Rosa, Corby Rosset, Sambudha Roy, Olatunji Ruwase, Olli Saarikivi, Amin Saied, Adil Salim, Michael Santacrose, Shital Shah, Ning Shang, Hiteshi Sharma, Yelong Shen, Swadheen Shukla, Xia Song, Masahiro Tanaka, Andrea Tupini, Praneetha Vaddamanu, Chunyu Wang, Guanhua Wang, Lijuan Wang, Shuohang Wang, Xin Wang, Yu Wang, Rachel Ward, Wen Wen, Philipp Witte, Haiping Wu, Xiaoxia Wu, Michael Wyatt, Bin Xiao, Can Xu, Jiahang Xu, Weijian Xu, Jilong Xue, Sonali Yadav, Fan Yang, Jianwei Yang, Yifan Yang, Ziyi Yang, Donghan Yu, Lu Yuan, Chenruidong Zhang, Cyril Zhang, Jianwen Zhang, Li Lyna Zhang, Yi Zhang, Yue Zhang, Yunan Zhang, and Xiren Zhou. Phi-3 technical report: A highly capable language model locally on your phone. *arXiv preprint*, 2024.
- [Adeniji *et al.*, 2023] Ademi Adeniji, Amber Xie, Carmelo Sferrazza, Younggyo Seo, Stephen James, and Pieter Abbeel. Language reward modulation for pretraining reinforcement learning, 2023.
- [Bai *et al.*, 2022] Yuntao Bai, Saurav Kadavath, Sandipan Kundu, Amanda Askell, Jackson Kernion, Andy Jones, Anna Chen, Anna Goldie, Azalia Mirhoseini, Cameron McKinnon, Carol Chen, Catherine Olsson, Christopher Olah, Danny Hernandez, Dawn Drain, Deep Ganguli, Dustin Li, Eli Tran-Johnson, Ethan Perez, Jamie Kerr, Jared Mueller, Jeffrey Ladish, Joshua Landau, Kamal Ndousse, Kamile Lukosuite, Liane Lovitt, Michael Sellitto, Nelson Elhage, Nicholas Schiefer, Noemi Mercado, Nova DasSarma, Robert Lasenby, Robin Larson, Sam Ringer, Scott Johnston, Shauna Kravec, Sheer El Showk, Stanislav Fort, Tamera Lanham, Timothy Telleen-Lawton, Tom Conerly, Tom Henighan, Tristan Hume, Samuel R. Bowman, Zac Hatfield-Dodds, Ben Mann, Dario Amodei, Nicholas Joseph, Sam McCandlish, Tom Brown, and Jared Kaplan. Constitutional ai: Harmlessness from ai feedback. *arXiv preprint arXiv:2212.08073*, 2022.
- [Baumli *et al.*, 2024] Kate Baumli, Satinder Baveja, Feryal Behbahani, Harris Chan, Gheorghe Comanici, Sebastian Flennerhag, Maxime Gazeau, Kristian Holsheimer, Dan Horgan, Michael Laskin, Clare Lyle, Hussain Masoom, Kay McKinney, Volodymyr Mnih, Alexander Neitz, Dmitry Nikulin, Fabio Pardo, Jack Parker-Holder, John Quan, Tim Rocktäschel, Himanshu Sahni, Tom Schaul, Yannick Schroecker, Stephen Spencer, Richie Steigerwald, Luyu Wang, and Lei Zhang. Vision-language models as a source of rewards, 2024.
- [Bradley and Terry, 1952] Ralph Allan Bradley and Milton E Terry. Rank analysis of incomplete block designs: I. the method of paired comparisons. *Biometrika*, 39(3/4):324–345, 1952.
- [Brockman *et al.*, 2016] Greg Brockman, Vicki Cheung, Ludwig Pettersson, Jonas Schneider, John Schulman, Jie Tang, and Wojciech Zaremba. Openai gym, 2016.
- [Bromley *et al.*, 1993] Jane Bromley, Isabelle Guyon, Yann LeCun, Eduard Säcker, and Roopak Shah. Signature verification using a "siamese" time delay neural network. In *Advances in Neural Information Processing Systems*, 1993.
- [Chen *et al.*, 2025] Zhe Chen, Weiyun Wang, Yue Cao, Yangzhou Liu, Zhangwei Gao, Erfei Cui, Jinguo Zhu, Shenglong Ye, Hao Tian, Zhaoyang Liu, Lixin Gu, Xuehui Wang, Qingyun Li, Yiming Ren, Zixuan Chen, Jiapeng Luo, Jiahao Wang, Tan Jiang, Bo Wang, Conghui He, Botian Shi, Xingcheng Zhang, Han Lv, Yi Wang, Wenqi Shao, Pei Chu, Zhongying Tu, Tong He, Zhiyong Wu, Huipeng Deng, Jiaye Ge, Kai Chen, Kaipeng Zhang, Limin Wang, Min Dou, Lewei Lu, Xizhou Zhu, Tong Lu, Dahua Lin, Yu Qiao, Jifeng Dai, and Wenhui Wang. Expanding performance boundaries of open-source multimodal models with model, data, and test-time scaling, 2025.

- [Christiano *et al.*, 2017] Paul Christiano, Jan Leike, Tom B. Brown, Miljan Martic, Shane Legg, and Dario Amodei. Deep reinforcement learning from human preferences. In *Advances in Neural Information Processing Systems*, volume 30. Curran Associates, Inc., 2017.
- [Chu *et al.*, 2023] Kun Chu, Xufeng Zhao, Cornelius Weber, Mengdi Li, and Stefan Wermter. Accelerating reinforcement learning of robotic manipulations via feedback from large language models, 2023.
- [Cui *et al.*, 2022] Yuchen Cui, Scott Niekum, Abhinav Gupta, Vikash Kumar, and Aravind Rajeswaran. Can foundation models perform zero-shot task specification for robot manipulation? In *Learning for Dynamics and Control Conference (LADC)*, 2022.
- [DeepMind, 2024] Google DeepMind. Gemini 2.0: Introducing our new ai model for the agentic era. <https://blog.google/technology/google-deepmind/google-gemini-ai-update-december-2024/>, 2024.
- [Du *et al.*, 2023] Yuqing Du, Olivia Watkins, Zihan Wang, Cédric Colas, Trevor Darrell, Pieter Abbeel, Abhishek Gupta, and Jacob Andreas. Guiding pretraining in reinforcement learning with large language models. In *Proceedings of the 40th International Conference on Machine Learning*, 2023.
- [Fan *et al.*, 2022] Linxi Fan, Guanzhi Wang, Yunfan Jiang, Ajay Mandlekar, Yuncong Yang, Haoyi Zhu, Andrew Tang, De-An Huang, Yuke Zhu, and Anima Anandkumar. Minedojo: Building open-ended embodied agents with internet-scale knowledge. In *Thirty-sixth Conference on Neural Information Processing Systems Datasets and Benchmarks Track*, 2022.
- [Fu *et al.*, 2024] Yuwei Fu, Haichao Zhang, Di Wu, Wei Xu, and Benoit Boulet. Furl: Visual-language models as fuzzy rewards for reinforcement learning. In *Proceedings of the 41st International Conference on Machine Learning*, 2024.
- [Ghosh *et al.*, 2025] Udita Ghosh, Dripta S. Raychaudhuri, Jiachen Li, Konstantinos Karydis, and Amit Roy-Chowdhury. Preference vlm: Leveraging vlms for scalable preference-based reinforcement learning, 2025.
- [Gupta *et al.*, 2022] Abhishek Gupta, Aldo Pacchiano, Yuxiang Zhai, Sham Kakade, and Sergey Levine. Unpacking reward shaping: Understanding the benefits of reward engineering on sample complexity. In *Advances in Neural Information Processing Systems*, 2022.
- [Haarnoja *et al.*, 2017] Tuomas Haarnoja, Aurick Zhou, Pieter Abbeel, and Sergey Levine. Soft actor-critic: Off-policy maximum entropy deep reinforcement learning with a stochastic actor. <https://arxiv.org/abs/1801.01290>, 2017.
- [Ibarz *et al.*, 2018] Borja Ibarz, Jan Leike, Tobias Pohlen, Geoffrey Irving, Shane Legg, and Dario Amodei. Reward learning from human preferences and demonstrations in atari. In *Advances in Neural Information Processing Systems*, 2018.
- [Jiang *et al.*, 2024] Haobin Jiang, Junpeng Yue, Hao Luo, Ziluo Ding, and Zongqing Lu. Reinforcement learning friendly vision-language model for minecraft. In *European Conference on Computer Vision (ECCV)*, 2024.
- [Kaelbling *et al.*, 1998] Leslie Pack Kaelbling, Michael L. Littman, and Anthony R. Cassandra. Planning and acting in partially observable stochastic domains. *Artificial Intelligence*, 101(1):99–134, 1998.
- [Klissarov *et al.*, 2023] Martin Klissarov, Pierluca D’Oro, Shagun Sodhani, Roberta Raileanu, Pierre-Luc Bacon, Pascal Vincent, Amy Zhang, and Mikael Henaff. Motif: Intrinsic motivation from artificial intelligence feedback. *arXiv preprint arXiv:2310.00166*, 2023.
- [Kwon *et al.*, 2023] Minae Kwon, Sang Michael Xie, Kalesha Bullard, and Dorsa Sadigh. Reward design with language models. In *International Conference on Learning Representations (ICLR)*, 2023.
- [Laud, 2004] Adam Daniel Laud. *Theory and application of reward shaping in reinforcement learning*. PhD thesis, University of Illinois at Urbana-Champaign, USA, 2004. AAI3130966.
- [Lee *et al.*, 2021a] Kimin Lee, Laura Smith, and Pieter Abbeel. Pebble: Feedback-efficient interactive reinforcement learning via relabeling experience and unsupervised pre-training. In *International Conference on Machine Learning*, 2021.
- [Lee *et al.*, 2021b] Kimin Lee, Laura Smith, Anca Dragan, and Pieter Abbeel. B-pref: Benchmarking preference-based reinforcement learning. *arXiv preprint arXiv:2111.03026*, 2021.
- [Leike *et al.*, 2018] Jan Leike, David Krueger, Tom Everitt, Miljan Martic, Vishal Maini, and Shane Legg. Scalable agent alignment via reward modeling: a research direction, 2018.
- [Lin *et al.*, 2020] Xingyu Lin, Yufei Wang, Jake Olkin, and David Held. Softgym: Benchmarking deep reinforcement learning for deformable object manipulation. In *Conference on Robot Learning*, 2020.
- [Liu *et al.*, 2025] Runze Liu, Chenjia Bai, Jiafei Lyu, Shengjie Sun, Yali Du, and Xiu Li. Vlp: Vision-language preference learning for embodied manipulation, 2025.
- [Ma *et al.*, 2023] Yecheng Jason Ma, William Liang, Vaidehi Som, Vikash Kumar, Amy Zhang, Osbert Bastani, and Dinesh Jayaraman. Liv: Language-image representations and rewards for robotic control. *arXiv preprint arXiv:2306.00958*, 2023.
- [Ma *et al.*, 2024] Yecheng Jason Ma, William Liang, Guanzhi Wang, De-An Huang, Osbert Bastani, Dinesh Jayaraman, Yuke Zhu, Linxi Fan, and Anima Anandkumar. Eureka: Human-level reward design via coding large language models, 2024.
- [Mahmoudieh *et al.*, 2022] Parsa Mahmoudieh, Sayna Ebrahimi, Deepak Pathak, and Trevor Darrell. Zero-shot reward specification via grounded natural language, 2022.

- [Nam *et al.*, 2023] Taewook Nam, Juyong Lee, Jesse Zhang, Sung Ju Hwang, Joseph J. Lim, and Karl Pertsch. Lift: Unsupervised reinforcement learning with foundation models as teachers, 2023.
- [OpenAI, 2019] OpenAI. Dota 2 with large scale deep reinforcement learning, 2019.
- [OpenAI, 2025] OpenAI. Introducing gpt-4.1 in the api. <https://openai.com/index/gpt-4-1/>, 2025. Accessed: 2025-05-07.
- [OpenBMB, 2025] OpenBMB. Minicpm-o 2.6: A gpt-4o-level mllm for vision, speech, and multimodal live streaming on your phone, 2025. Accessed: 2025-05-07.
- [Palo *et al.*, 2023] Norman Di Palo, Arunkumar Byravan, Leonard Hasenclever, Markus Wulfmeier, Nicolas Heess, and Martin Riedmiller. Towards a unified agent with foundation models, 2023.
- [Radford *et al.*, 2021] Alec Radford, Jong Wook Kim, Chris Hallacy, Aditya Ramesh, Gabriel Goh, Sandhini Agarwal, Girish Sastry, Amanda Askell, Pamela Mishkin, Jack Clark, Gretchen Krueger, and Ilya Sutskever. Learning transferable visual models from natural language supervision. In *Proceedings of the 38th International Conference on Machine Learning*, 2021.
- [Rocamonde *et al.*, 2024] Juan Rocamonde, Victoriano Montesinos, Elvis Nava, Ethan Perez, and David Lindner. Vision-language models are zero-shot reward models for reinforcement learning. In *The Twelfth International Conference on Learning Representations*, 2024.
- [Schulman *et al.*, 2017] John Schulman, Filip Wolski, Prafulla Dhariwal, Alec Radford, and Oleg Klimov. Proximal policy optimization algorithms, 2017.
- [Sontakke *et al.*, 2023] Saurabh A Sontakke, Jiapeng Zhang, Spencer Arnold, Karl Pertsch, Emre Biyik, Dorsa Sadigh, Chelsea Finn, and Laurent Itti. Roboclip: One demonstration is enough to learn robot policies. In *Thirty-seventh Conference on Neural Information Processing Systems (NeurIPS)*, 2023.
- [Team, 2025a] Gemma Team. Gemma 3, 2025.
- [Team, 2025b] Qwen Team. Qwen2.5-vl, January 2025.
- [Venkataraman *et al.*, 2024] Sreyas Venkataraman, Yufei Wang, Ziyu Wang, Zackory Erickson, and David Held. Real-world offline reinforcement learning from vision language model feedback, 2024.
- [Wang *et al.*, 2023a] Guanzhi Wang, Yuqi Xie, Yunfan Jiang, Ajay Mandlekar, Chaowei Xiao, Yuke Zhu, Linxi Fan, and Anima Anandkumar. Voyager: An open-ended embodied agent with large language models. *arXiv preprint arXiv: Arxiv-2305.16291*, 2023.
- [Wang *et al.*, 2023b] Yufei Wang, Zhou Xian, Feng Chen, Tsun-Hsuan Wang, Yian Wang, Katerina Fragkiadaki, Zackory Erickson, David Held, and Chuang Gan. Robogen: Towards unleashing infinite data for automated robot learning via generative simulation. *arXiv preprint arXiv:2311.01455*, 2023.
- [Wang *et al.*, 2024] Yufei Wang, Zhanyi Sun, Jesse Zhang, Zhou Xian, Erdem Biyik, David Held, and Zackory Erickson. RL-vlm-f: Reinforcement learning from vision language foundation model feedback. In *Proceedings of the 41st International Conference on Machine Learning*, 2024.
- [Wu *et al.*, 2024] Zhiyu Wu, Xiaokang Chen, Zizheng Pan, Xingchao Liu, Wen Liu, Damai Dai, Huazuo Gao, Yiyang Ma, Chengyue Wu, Bingxuan Wang, Zhenda Xie, Yu Wu, Kai Hu, Jiawei Wang, Yaofeng Sun, Yukun Li, Yishi Piao, Kang Guan, Aixin Liu, Xin Xie, Yuxiang You, Kai Dong, Xingkai Yu, Haowei Zhang, Liang Zhao, Yisong Wang, and Chong Ruan. Deepseek-vl2: Mixture-of-experts vision-language models for advanced multimodal understanding, 2024.
- [Xie *et al.*, 2024] Tianbao Xie, Siheng Zhao, Chen Henry Wu, Yitao Liu, Qian Luo, Victor Zhong, Yanchao Yang, and Tao Yu. Text2reward: Reward shaping with language models for reinforcement learning. In *The Twelfth International Conference on Learning Representations*, 2024.
- [Yu *et al.*, 2019] Tianhe Yu, Deirdre Quillen, Zhanpeng He, Ryan Julian, Avnish Narayan, Hayden Shively, Adithya Bellathur, Karol Hausman, Chelsea Finn, and Sergey Levine. Meta-world: A benchmark and evaluation for multi-task and meta reinforcement learning. In *Conference on Robot Learning (CoRL)*, 2019.
- [Yu *et al.*, 2023] Wenhao Yu, Nimrod Gileadi, Chuyuan Fu, Sean Kirmani, Kuang-Huei Lee, Montse Gonzalez Arenas, Hao-Tien Lewis Chiang, Tom Erez, Leonard Hasenclever, Jan Humplik, Brian Ichter, Ted Xiao, Peng Xu, Andy Zeng, Tingnan Zhang, Nicolas Heess, Dorsa Sadigh, Jie Tan, Yuval Tassa, and Fei Xia. Language to rewards for robotic skill synthesis. *arXiv preprint arXiv:2306.08647*, 2023.

## A VLM

### A.1 Prompts

To evaluate VLM prompting strategies, we crafted three prompt templates of increasing reasoning complexity:

- **S1 — Single Stage**

1. The goal is  $\{task\_description\}$ . Is the goal better achieved in Image 1 or Image 2? Relay a single line of 1 if the goal is better achieved in Image 1, or 2 if it is better achieved in Image 2. Reply 0 if the text is unsure or there is no difference.

- **S2 — Two Stages**

1. The goal is  $\{task\_description\}$ . Is the goal better achieved in Image 1 or Image 2?
2. Based on the text above, Relay a single line of 1 if the goal is better achieved in Image 1, or 2 if it is better achieved in Image 2. Reply 0 if the text is unsure or there is no difference.

- **S2 + CoT — Two Stages with Chain-of-Thought**

1. – What is shown in Image 1?  
– What is shown in Image 2?  
– The goal is  $\{<task\_description\}$ . Is there any difference between Image 1 and Image 2 in terms of achieving the goal?
2. Same as S2 Stage 2.

- **S1<sub>2</sub> — Single Stages (Binary)**

1. The goal is  $\{task\_description\}$ . Is Image 2 more likely to achieve the goal? Reply a single line of 1 if yes, otherwise 0.

- **S2<sub>2</sub> — Two Stages (Binary)**

1. The goal is  $\{task\_description\}$ . Is Image 2 more likely to achieve the goal?
2. Based on the text above, Reply a single line of 1 if yes, otherwise 0.

#### Rationale.

- **Single-Stage (S1).** The VLM is asked to output only a categorical label. This setting measures the model’s raw decision quality without exposing its reasoning.
- **Two-Stage (S2).** We first solicit an *open-ended answer* that explains *why* the goal is better achieved in one image. The model then self-produces the final label in Stage 2. Recording Stage 1 lets us inspect the model’s internal rationale and assess whether it is aligned with the label it finally assigns.

Table 3: Impact of prompt design on VLM accuracy across ten tasks (higher is better).

Model	Prompt	CartPole	Straighten Rope	Pass Water	Soccer	Sweep Into	Drawer Open	Combat Spider	Milk Cow	Sheep	Hunt Cow
MiniCPM-o-2.6	S1 <sub>2</sub>	0.50	0.64	0.50	0.65	0.79	0.56	0.59	0.77	0.57	0.64
	S2 <sub>2</sub>	0.45	0.61	0.54	0.80	0.61	0.64	0.65	0.61	0.65	0.62
	S1	0.50	0.60	0.44	0.53	0.54	0.60	0.53	0.72	0.72	0.53
	S2	0.52	0.50	0.54	0.53	0.73	0.60	0.65	0.70	0.58	0.70
Phi-3.5	S2 + CoT	0.53	0.61	0.73	0.63	0.55	0.76	<b>0.82</b>	0.76	0.62	0.72
	S1 <sub>2</sub>	0.50	0.59	0.50	0.52	0.69	0.54	0.63	<b>0.90</b>	<b>0.90</b>	0.66
	S2 <sub>2</sub>	0.76	0.50	0.47	0.50	0.75	0.53	0.66	0.83	0.89	0.68
	S1	0.68	0.67	0.62	0.51	0.60	0.43	0.62	0.58	0.76	0.66
GPT-4.1-nano	S2	0.50	0.63	0.55	0.54	0.50	0.52	0.58	0.62	0.76	0.59
	S2 + CoT	0.56	0.61	0.56	0.45	0.46	0.51	0.59	0.66	0.72	0.64
	S1	0.48	0.50	0.49	0.84	0.50	0.51	0.58	0.59	0.60	0.53
	S2	0.43	0.67	0.58	0.50	0.50	0.41	0.49	0.58	0.62	0.59
Gemini-2.0	S2 + CoT	0.66	0.81	0.65	0.60	0.81	0.65	0.64	0.62	0.66	0.66
	S1	<b>0.91</b>	0.82	0.58	0.73	<b>0.87</b>	<b>0.84</b>	<b>0.82</b>	0.78	0.80	0.76
	S2	0.86	<b>0.87</b>	0.59	0.61	<b>0.87</b>	0.64	0.72	0.78	0.79	0.73
	S2 + CoT	<b>0.91</b>	0.84	<b>0.70</b>	<b>0.87</b>	<b>0.87</b>	<b>0.84</b>	0.62	0.76	0.77	<b>0.76</b>

Table 4: Details of the VLMs we benchmarked on an RTX 3090 (float16, batch = 1, prompt S1).

Model	Params (B)	VRAM (GB)	Latency (s/query)
Phi-3.5-Vision-Instruct	4.15	10	0.38
MiniCPM-o-2.6	8.67	18	0.34
DeepSeek-VL2-Tiny	3.37	16	0.20
Qwen2.5-VL-7B-Instruct	8.29	16	0.25
InternVL2.5-8B	8.08	21	1.17
Gemma-3-12b-it	12.2	22	10.36
CLIP (ViT-L/14@336px)	0.43	1	0.03
MineCLIP (Attn)	0.16	2	0.02

- **Two-Stage + CoT (S2 + CoT).** Stage 1 is further broken into three fixed sub-questions (*describe Image 1, describe Image 2, compare w.r.t. the goal*). This *structured Chain-of-Thought* (CoT) explicitly guides the model to observe, compare, and reason step-by-step before emitting the label in Stage 2, reducing the chance of shortcut reasoning.
- **Binary (S1<sub>2</sub> and S2<sub>2</sub>).** The VLM is required to output a *binary* label (0 or 1). Empirically, we find that some models perform better when the prompt is kept as simple as possible.

### A.2 VLM accuracy

**Evaluation Protocol.** For each task we curate 100 image pairs with *pseudo* ground-truth preference labels:

- **50 pairs** in which Image 2 represents an improvement over Image 1 (label = 1), and
- **50 pairs** in which it does not (label = 0).<sup>1</sup>

The VLM’s raw prediction  $y \in \{0, 1, 2\}$  is post-processed by

$$\hat{y} = \max(y - 1, 0),$$

so that

- $y = 2$  (*Image 2 better*)  $\longrightarrow \hat{y} = 1$ , and
- $y \in \{0, 1\}$  (*unsure/no difference or Image 1 better*)  $\longrightarrow \hat{y} = 0$ .

We then compare  $\hat{y}$  with the pseudo ground-truth label for accuracy and other downstream metrics.

Table 3 summarizes the performance of different prompt designs evaluated across multiple models. We observed

<sup>1</sup>Label 0 subsumes both “Image 1 is better than Image 2” and “the two images are indistinguishable w.r.t. the goal.”

Table 5: Siamese reward-model architecture. A shared CNN maps every input image to a 128-D embedding; the two embeddings are concatenated and processed by an MLP head that outputs two logits.

# / Stage	Layer	Specification	Activation
<i>Shared encoder (per image)</i>			
1–6	Custom CNN	see Table 9 (128-D)	ReLU, Tanh
<i>Comparison head (MLP, takes <math>256 = 128 \times 2</math>-D)</i>			
7	Linear	256→64	ReLU
8	Linear	64→2	—

that for **Gemini 2.0**, even the simplest prompt design (S1) yielded strong performance. In contrast, **GPT-4.1-nano** performed better with the slightly more elaborate S2 prompt, and showed further improvements in accuracy with Chain-of-Thought prompting (S2 + CoT). Interestingly, **Phi-3.5** exhibited the opposite trend in MineDojo-style tasks, favoring simpler prompts—achieving the best results with **S1<sub>2</sub>**, a binary decision format with a single-stage comparison.

As a result, in all subsequent experiments, we adopt the following prompt configuration per model:

- **Gemini 2.0** and **MiniCPM** use **S1**,
- **Phi-3.5** uses **S1<sub>2</sub>**.

Table 4 provides detailed statistics on computational resources and runtime used for evaluating each model.

## B Hyper-parameters and Network Architectures

### B.1 Relative Reward Model (Siamese)

#### Architecture

The overall architecture of the Siamese model is summarized in Table 5. Each image is first processed by a *shared* CNN encoder that produces a 128-dimensional embedding. The two embeddings are concatenated and passed through a fully connected layer with 64 hidden units, followed by a final linear layer that outputs a two-dimensional logits vector indicating the preference direction (e.g., *regression* vs. *improvement*). Because the Siamese architecture is inherently symmetric, we relabel  $y = -1$  (“equally preferable” or “incomparable”) to  $y = 0$  during training, resulting in a binary target  $y \in \{0, 1\}$ .

#### Training Details.

- **Loss**: cross-entropy on the two-class logits
- **Ensemble**: three independently initialized Siamese models; their softmax outputs are averaged at inference for greater robustness
- **Sampling strategy**: uniform from the replay buffer
- **Sampling frequency**: 50 pairs per 1 000 environment steps
- **Buffer capacity**: 500 000 transition pairs
- **Training frequency**: 50 gradient updates per 1 000 environment steps
- **Batch size**: 32

Table 6: Tasks, simulation suites, and goal prompts used in our experiments.

Suite	Task ID	Goal prompt supplied to the VLM
Gym	CartPole	balance the brown pole on the black cart to be upright
SoftGym	Straighten Rope	straighten the blue rope
	Pass Water	move the container that holds water as close to the red circle as possible without spilling
MetaWorld	Soccer	minimise the distance between the soccer ball and the goal
	Sweep Into Drawer	minimise the distance between the green cube and the hole
	Open	maximise drawer opening
MineDojo	Combat Spider	combat a spider
	Milk Cow	milk a cow
	Shear Sheep	shear a sheep
	Hunt Cow	hunt a cow

Table 7: Goal prompts fed to CLIP and MineCLIP encoders.

Suite	Task ID	CLIP/MineCLIP prompt
Gym	CartPole	pole vertically upright on top of the cart.
SoftGym	Straighten Rope	The blue rope is straightened.
	Pass Water	The container, which holds water, is as close to the red circle as possible without causing too many water droplets to spill.
MetaWorld	Soccer	The soccer ball is in the goal.
	Sweep Into Drawer	The green cube is in the hole.
	Open	The drawer is opened.
MineDojo	Combat Spider	combat a spider
	Milk Cow	milk a cow
	Shear Sheep	shear a sheep
	Hunt Cow	hunt a cow

## B.2 Policy model

### MineDojo tasks.

- **Framework**: `stable-baselines3` — Proximal Policy Optimization (PPO)
- **Network**: frozen MineCLIP image encoder → MLP(64, 64)
- **Entropy coefficient**: 0.01
- **Other parameters**: default
- **Vectorised environment**: `DummyVecEnv` with 4 workers
- **Observation wrapper**: 4-frame stack

### Other tasks.

- **Framework**: modified `RL-VLM-F` — Soft Actor-Critic (SAC)
- **Network**: 3 hidden layers  $\times$  256 units, `tanh` activations (actor & critic)
- **Learning rates**:  $3 \times 10^{-4}$  for both actor and critic
- **Batch size**: 512
- **Replay buffer**: 500 000 transitions

## B.3 Compute Resources

All experiments were conducted on NVIDIA L40 GPUs with 48GB memory. We also verified that all experiments can be reproduced on NVIDIA RTX 3090 GPUs with 24GB memory. Each experiment run with a single seed can typically be completed within 24 hours. By training a Siamese relative reward model, our scheduling strategy reduces the number of VLM queries during policy learning by approximately  $20 \times$  compared to direct VLM querying at rollout time.

## C Details on Tasks and Environments

We benchmark our approach on ten goal-conditioned control tasks drawn from four simulators: GYM, SOFTGYM, METAWORLD, and MINEDOJO. The tasks are as follows.

- **CartPole**: Balance an upright pole on a moving cart.

Table 8: Observation modalities, action spaces, and episode horizons for all evaluated tasks.

Suite	Task(s)	Observation	Action space	Horizon
Gym	CartPole	4-D state $(x, \dot{x}, \theta, \dot{\theta})$	$\text{Box}([0, 1])$ - scalar torque	100
SoftGym	Straighten Rope	36-D particle positions	picker - 2 grippers, 6-D $\Delta$ position	40 (rep=6)
	Pass Water	7-D state (container size 3, target pos 1, water-height 1, water-in/out 2)	$\text{Box}(\mathbb{R}^1)$ - $\Delta$ pos along constrained axis	75 (rep=8)
MetaWorld	Soccer, Sweep Into, Drawer Open	39-D proprioceptive state (arm 3 + gripper 1 + object 14 + history 18 + goal 3)	$\text{Box}(\mathbb{R}^3)$ - $\Delta x, y, z$ + gripper open/close	500
MineDojo	Combat Spider, Milk Cow, Shear Sheep, Hunt Cow	RGB 126×256×3 (first-person)	$\text{MultiDiscrete}([12, 3])$ - 12 camera/locomotion, 3 mouse magnitudes	500

- **Straighten Rope:** Straighten a rope from a randomly tangled configuration.
- **Pass Water:** Move a glass of water to a target location without spilling its contents.
- **Open Drawer:** Use a robotic arm to pull open a drawer on a desk.
- **Soccer:** Push a soccer ball into a designated goal area using a robotic arm.
- **Sweep Into:** Sweep a green cube into a hole on the table using a robotic arm.
- **Combat Spider:** Eliminate a spider in combat. The agent is initialized with a diamond sword, a shield, full diamond armor, and a nearby spider.
- **Milk Cow:** Find and approach a cow, then collect milk using an empty bucket. The agent is initialized with a bucket, and a cow is spawned nearby.
- **Shear Sheep:** Find and approach a sheep, then collect its wool using a shear. The agent starts with a shear and a sheep nearby.
- **Hunt Cow:** Find and approach a cow, then hunt it using a sword. The cow will attempt to flee, requiring the agent to chase it down. The agent is initialized with a diamond sword and a cow nearby.

For each task we hand-craft a concise natural-language *goal prompt* that is fed into the VLM during preference querying (see Appendix A.1). Table 6 summarizes the task IDs and the exact goal prompts. For image–language models based on *frozen* CLIP or MineCLIP encoders we supply a different set of goal descriptions phrased as *achievement statements*. Table 7 lists the exact prompts; The prompts adopt a declarative “goal achieved” style (e.g. “*The drawer is opened.*”) that is empirically more compatible with the image–text contrastive objectives. Table 8 summarises the observation modality, action space, and episode horizon of each task.

#### Additional notes:

- *Straighten Rope*: two end-point pickers are pre-grasped at reset; the 6-D action is the 3-D  $\Delta$  position of each picker.
- *Pass Water*: the glass container moves along a single horizontal axis, resulting in a 1-D action.
- *MetaWorld tasks*: we initialise the gripper close to the target object and re-align the camera such that the object is centred, producing cleaner images for the VLM.

Table 9: Custom CNN backbone.

#	Layer	Specification (kernel / stride)	Activation
1	Conv2d 3→16	5×5 / 3	ReLU
2	Conv2d 16→32	3×3 / 2	ReLU
3	Conv2d 32→64	3×3 / 2	ReLU
4	Conv2d 64→128	3×3 / 2	ReLU
5	Flatten	—	—
6	Linear 512→1	—	Tanh

Table 10: ResNet-18 backbone used in RL-VLM-F baselines.

Stage	Layer / Block	Specification	Activation
0	Conv1	7×7, 64, stride 2 + MaxPool	ReLU
1	Layer1	BasicBlock, 64 × 2	ReLU
2	Layer2	BasicBlock, 128 × 2	ReLU
3	Layer3	BasicBlock, 256 × 2	ReLU
4	Layer4	BasicBlock, 512 × 2	ReLU
5	AvgPool	AdaptiveAvgPool2d (1×1)	—
6	FC head	Linear 512→1	—

- *MineDojo tasks*: observations are limited to first-person RGB frames only (no yaw, pitch, GPS, or voxel data) to better reflect real-world vision. We enable *fast reset* with random teleportation, fix the world seed to 123, and constrain the biome to SUNFLOWERPLAINS.

## D Details on Baselines

### D.1 VLM-AR3L (Ours)

In all experiments, we set the absolute reward weighting to  $\alpha = 0.5$ , the confidence threshold to  $\tau = 0.52$ , and the temporal offset to  $k = 16$ .

### D.2 RL-VLM-F

Released by [Wang *et al.*, 2024], RL-VLM-F employs two image–reward backbones that differ by environment suite:

- **Custom CNN:** Table 9; used for GYM and META-WORLD.
- **ResNet-18:** Table 10; used for SOFTGYM and MINE-DOJO.

**ResNet-18 Backbone (SoftGym & MineDojo).** A vanilla ResNet-18 ( $\text{BasicBlock} \times [2, 2, 2, 2]$ ) is adopted for high-variance visual inputs. ImageNet initialisation is retained, but the final FC layer is replaced with a 1- or 2-unit head.

**Training protocol.** Except for the backbone choice above, all optimisation hyper-parameters and data-collection schedules follow the settings described in Section B.1.

### D.3 CLIP

For image–language matching we use the original **OpenAI CLIP ViT-L/14 @ 336 px** checkpoint. During interaction we compute a *static* similarity reward at each step:

1. **Text embedding.** The goal prompt  $g$  is tokenised and encoded once; its feature vector is  $\ell_2$ -normalised.

Table 11: Shaped *dense* ground-truth reward for each task ( $\mathbb{1}[\cdot]$  is the indicator).

Task	Reward $r_t$
CartPole	$- \theta_t $
Straighten Rope	$\min(d_{\text{end}}(t), 1.1 L_{\text{rope}})$
Pass Water	$-\lambda_{\text{spill}} \frac{w_{\text{out}}}{w_{\text{tot}}} - \lambda_{\text{dist}}  x_t - x_{\text{goal}} $
Soccer	$\max(\lambda_{\text{object}} \mathbb{I}[\text{ball grasped}] + \lambda_{\text{in-place}} \mathbb{I}[\text{ball in place}], \lambda_{\text{success}} \mathbb{I}[d_{\text{ball,goal}} < R_{\text{goal}}])$
Sweep Into	$\max(\lambda_{\text{object}} \mathbb{I}[\text{cube grasped}] + \lambda_{\text{in-place}} \mathbb{I}[\text{cube in hole}], \lambda_{\text{success}} \mathbb{I}[d_{\text{cube,hole}} < R_{\text{hole}}])$
Drawer Open	$\lambda_{\text{caging}} \cdot \text{caging} + \lambda_{\text{opening}} \cdot \text{opening}$
Combat Spider	$\lambda_{\text{attack}} \mathbb{I}[\text{valid attack}] + \lambda_{\text{success}} \mathbb{I}[\text{spider eliminated}]$
Milk Cow	$\lambda_{\text{nav}} \max(d_{\text{min},t-1} - d_{\text{min},t}, 0) + \lambda_{\text{success}} \mathbb{I}[\text{milk collected}]$
Shear Sheep	$\lambda_{\text{nav}} \max(d_{\text{min},t-1} - d_{\text{min},t}, 0) + \lambda_{\text{success}} \mathbb{I}[\text{sheep sheared}]$
Hunt Cow	$\lambda_{\text{attack}} \mathbb{I}[\text{valid attack}] + \lambda_{\text{nav}} \max(d_{\text{min},t-1} - d_{\text{min},t}, 0) + \lambda_{\text{success}} \mathbb{I}[\text{cow eliminated}]$

- Image embedding.** The current RGB observation is passed through the frozen CLIP image encoder, and  $\ell_2$ -normalised.
- Reward.** The cosine similarity  $r_t = \langle f_{\text{img}}, f_{\text{text}} \rangle$  is used directly as an reward (higher implies closer to the goal).

#### D.4 MineCLIP

For long-horizon visual tasks we employ the **MineCLIP-attn** reward model of [Fan *et al.*, 2022]. Its inference pipeline consists of three stages:

- Frame encoder** – each RGB frame is embedded by a frozen ViT-B/16 backbone.
- Temporal aggregator** – a 2-layer Transformer ( $d_{\text{model}}=512$ ) compresses the 16-frame sequence into a single video feature  $\in \mathbb{R}^F$ .
- Reward head** – an MLP takes the tokenised goal prompt and outputs a two-logit vector  $= [z_{\text{POS}}, z_{\text{NEG}}]$ ; the positive logit is taken as the scalar reward,  $r_t = z_{\text{POS}}$ .

#### Implementation notes.

- A sliding window stores the most recent 16 frames. Only when the window is full do we query MineCLIP; otherwise the reward is set to 0.
- Input frames are normalised with the official MineCLIP statistics  $(\mu, \sigma)$ .

#### D.5 GT Dense Reward (Oracle)

For ablation-style oracle comparisons, we define shaped dense rewards (Table 11) along with their task-specific weighting coefficients (Table 12). The meaning of each variable used in these reward definitions is provided in Table 13.

#### D.6 GT Sparse Reward (Oracle)

Sparse rewards remove shaped terms and give a single bonus  $r_t = \lambda_{\text{success}} \mathbb{I}[\text{task success}]$  (Table 14).

## E Additional Experimental Results

### E.1 Ablation Hyper-parameters

We conduct ablation studies on the temporal offset  $k$  and the weighting coefficient  $\alpha$ . As shown in Fig. 9, varying  $k$  does not result in significant performance differences, indicating that our method is relatively insensitive to the choice of temporal offset. Fig. 10 investigates the weighting coefficient  $\alpha$

Table 12: Non-zero coefficients  $\lambda$  for the dense rewards. Tasks not listed (CartPole, Straighten Rope) have no tunable  $\lambda$ .

Task	Coefficients
Pass Water	$\lambda_{\text{spill}}=10, \lambda_{\text{dist}}=1$
Soccer	$\lambda_{\text{object}}=3, \lambda_{\text{in-place}}=6.5, \lambda_{\text{success}}=10$
Sweep Into	$\lambda_{\text{object}}=2, \lambda_{\text{in-place}}=6, \lambda_{\text{success}}=10$
Drawer Open	$\lambda_{\text{caging}}=5, \lambda_{\text{opening}}=5$
Combat Spider	$\lambda_{\text{attack}}=1, \lambda_{\text{success}}=10$
Milk Cow	$\lambda_{\text{nav}}=0.1, \lambda_{\text{success}}=10$
Shear Sheep	$\lambda_{\text{nav}}=0.1, \lambda_{\text{success}}=10$
Hunt Cow	$\lambda_{\text{attack}}=1, \lambda_{\text{nav}}=0.1, \lambda_{\text{success}}=10$

Table 13: Meaning of the variables used in dense-reward formulas.

Symbol	Description
$\theta_t$	Pole angle at time $t$ (CartPole). Zero means perfectly upright.
$d_{\text{end}}(t)$	Distance between the two rope end-points at time $t$ (Straighten Rope).
$L_{\text{rope}}$	Nominal (fully straight) rope length (Straighten Rope).
$w_{\text{out}}$	Number of water particles outside the glass (Pass Water).
$w_{\text{tot}}$	Total number of water particles (Pass Water).
$x_t$	Current $x$ -position of the glass (Pass Water).
$x_{\text{goal}}$	Target $x$ -position for the glass (Pass Water).
$d_{\text{ball,goal}}$	Euclidean distance from soccer ball to goal centre (Soccer).
$R_{\text{goal}}$	Acceptable radius around the goal centre (Soccer).
$d_{\text{cube,hole}}$	Distance from cube centre to hole centre (Sweep Into).
$R_{\text{hole}}$	Acceptable radius around the hole centre (Sweep Into).
<i>caging</i>	Tolerance-shaped reward encouraging the gripper TCP to cage the drawer handle (Drawer Open). Formally $\text{caging} = f(\ \mathbf{x}_{\text{grip}} - \mathbf{x}_{\text{handle}}\ )$ ; see <code>reward.utils.tolerance</code> .
<i>opening</i>	Tolerance-shaped reward for the handle’s displacement toward the fully-open target (Drawer Open).
$d_{\text{min},t}$	Shortest agent-to-animal distance at time $t$ (Milk Cow, Shear Sheep, Hunt Cow).
$\mathbb{1}[\cdot]$	Indicator function, equals 1 if the event inside the brackets is true, 0 otherwise.

Table 14: Success criteria and sparse-reward scale  $\lambda_{\text{success}}$ .

Task	Success condition	$\lambda_{\text{success}}$
CartPole	$ \theta_t  < 5^\circ$	1
Straighten Rope	$d_{\text{end}} > 0.95 L_{\text{rope}}$	1
Pass Water	Dense reward $> -0.36$	1
Soccer	ball within $R_{\text{target}}$ of goal	1
Sweep Into	cube within $R_{\text{target}}$ of hole	1
Drawer Open	drawer opened beyond $R_{\text{target}}$	1
Combat Spider	spider eliminated	10
Milk Cow	milk collected	10
Shear Sheep	wool collected	10
Hunt Cow	cow eliminated	10

for the absolute reward signals. The method performs consistently well over a broad range of  $\alpha$ , while performance deteriorates only when extremely small or large values are used.

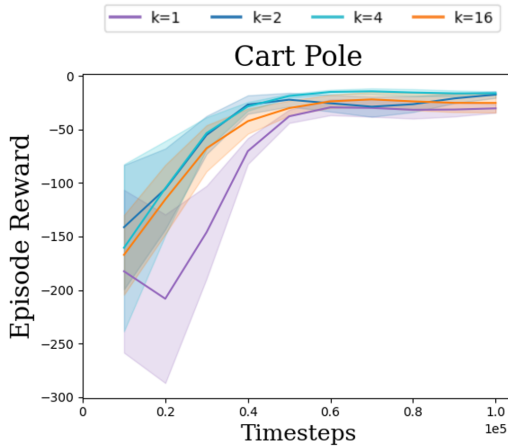


Figure 9: Ablation studies of temporal offset  $k$ .

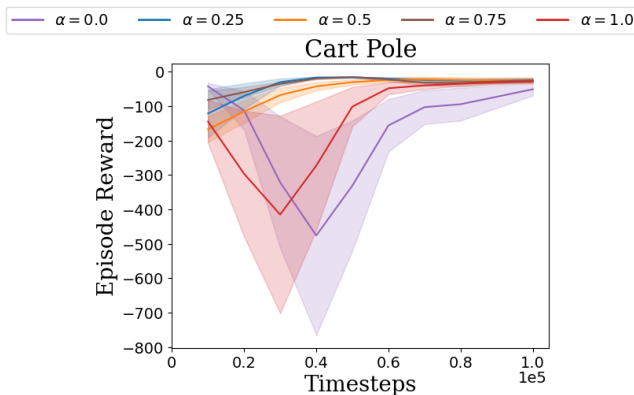


Figure 10: Ablation studies of weighting coefficient  $\alpha$ .

## E.2 Ablation VLM

See Figure 11 and Table 15. Our results show that Phi-3.5 exhibits strong performance in interpreting Minecraft-specific visual states. MiniCPM-o 2.6, on the other hand, performs competitively on more structured tasks such as Soccer and Drawer Open.

## E.3 Ablation Absolute and Relative rewards

See Figure 12. We compare three variants: absolute-only ( $\alpha=1$ ), relative-only ( $\alpha=0$ ), and the dual reward (default  $\alpha=0.5$ ). Absolute rewards tend to work well in tasks with a clear global progress measure, while relative rewards provide more reliable guidance in long-horizon or visually ambiguous tasks. Combining them yields the best or near-best performance in most tasks, supporting the complementarity discussed in Section 4.

## F Broader Impact

Our work leverages vision-language models (VLMs) to provide reward signals for reinforcement learning without requiring extensive manual reward engineering. This approach has several positive societal implications, including:

- **Reducing Development Costs:** By using pre-trained VLMs to generate rewards, we reduce the need for domain-specific reward design, potentially lowering the cost and effort required to train RL agents in complex or open-ended environments.
- **Scalability:** The method can be applied to various domains without extensive task-specific tuning, facilitating broader adoption of RL in areas like robotics, game environments, and simulation-based training.

However, there are also potential negative implications:

- **Bias Propagation:** If the VLMs used for reward labeling exhibit biases, these biases could be propagated to the RL agents, potentially leading to biased or harmful behaviors.
- **Unintended Applications:** The method could be exploited to train agents for undesirable purposes, such as manipulating environments to achieve harmful objectives or reinforcing negative behaviors.

To mitigate these risks, we recommend implementing bias detection mechanisms in VLM outputs and restricting the application of the trained RL agents to controlled and monitored environments. Additionally, transparency in VLM training procedures can further minimize potential harms.

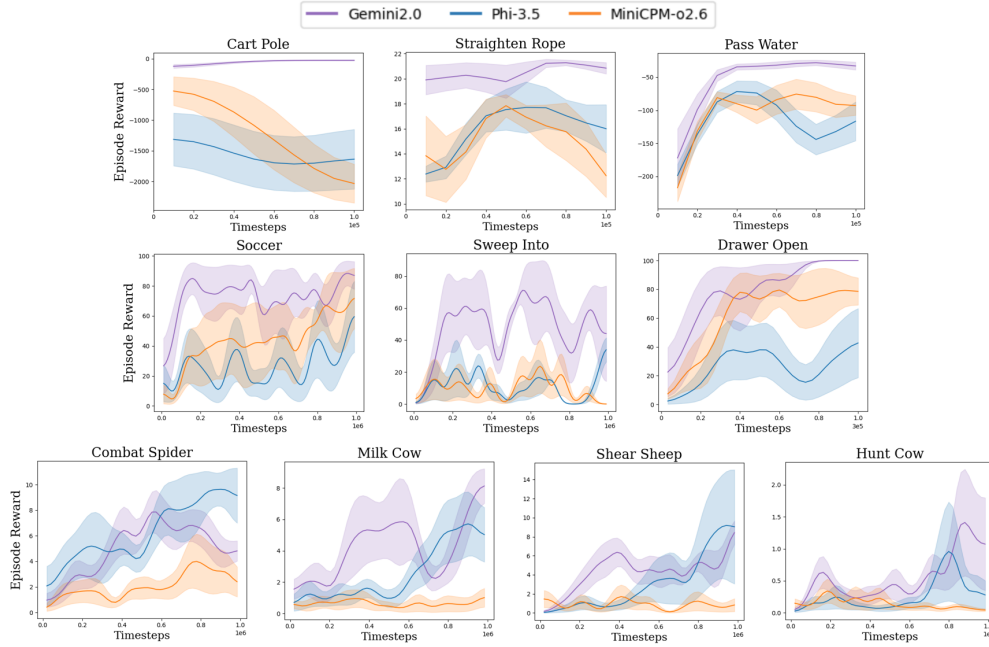


Figure 11: Ablation results with different vision-language models.

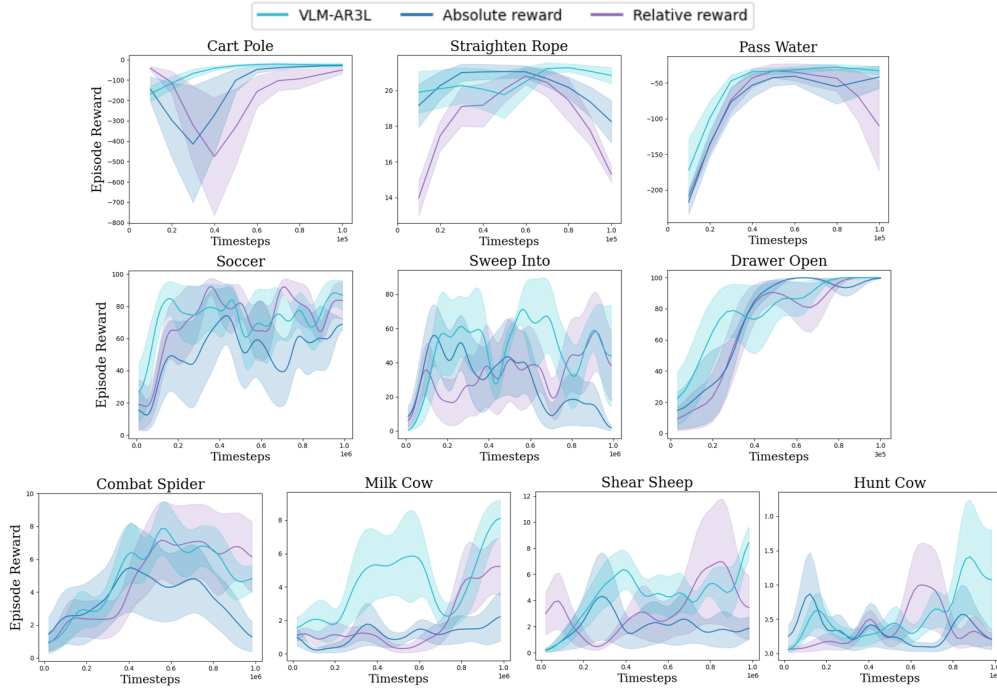


Figure 12: Ablation studies of absolute and relative rewards.

Table 15: Success rate (mean  $\pm$  standard error) of policy using difference VLM. Results are averaged over 3 random seeds with 5 evaluation episodes per best checkpoint.

Methods	CartPole	Straigten Rope	Pass Water	Soccer	Sweep Into	Drawer Open	Spider Combat	Milk Cow	Sheep Shear	Hunt Cow
Gemini2.0	<b>1.00 <math>\pm</math> 0.00</b>	<b>1.00 <math>\pm</math> 0.00</b>	<b>1.00 <math>\pm</math> 0.00</b>	<b>1.00 <math>\pm</math> 0.00</b>	<b>1.00 <math>\pm</math> 0.00</b>	<b>1.00 <math>\pm</math> 0.00</b>	<b>0.85 <math>\pm</math> 0.05</b>	<b>0.95 <math>\pm</math> 0.00</b>	<b>0.70 <math>\pm</math> 0.10</b>	<b>0.52 <math>\pm</math> 0.02</b>
Phi3.5	0.67 $\pm$ 0.47	1.00 $\pm$ 0.00	0.33 $\pm$ 0.47	1.00 $\pm$ 0.00	1.00 $\pm$ 0.00	1.00 $\pm$ 0.00	0.83 $\pm$ 0.13	0.81 $\pm$ 0.18	0.53 $\pm$ 0.34	0.37 $\pm$ 0.29
MiniCPM-o2.6	1.00 $\pm$ 0.00	1.00 $\pm$ 0.00	0.67 $\pm$ 0.47	1.00 $\pm$ 0.00	1.00 $\pm$ 0.00	1.00 $\pm$ 0.00	0.52 $\pm$ 0.23	0.43 $\pm$ 0.09	0.33 $\pm$ 0.19	0.19 $\pm$ 0.09